Report fluid-dynamic simulation of plume discharge for carbonate storage in deep sea

Diego Bindoni Antonella Abbà

August 23, 2023

Abstract

The aim of this paper is to collect and illustrate, for future collaborators or researchers, the work being carried out in recent months: to simulate the distribution of calcium bicarbonates in an oceanic environment, at depth, with the aim of storing the carbon dioxide absorbed from the atmosphere through a technological process developed and patented by LIMENET. The aim of the simulations will be to evaluate the distribution of the saturation state of the water Ω during a discharge cycle, in order to assess the probability of carbon dioxide reformation, thus studying a suitable discharge method to minimise the risk. The paper is intended as an illustration to understand the modelling choices made and the underlying assumptions, as well as the equations adopted, the simulated environment and the computational aspects of interest. Thanks are due to Professors Abbà, Caserini, Macchi and Raos of the Politecnico di Milano, who contributed to this project, as well as to PhD student Selene Varlerio.

Keywords: LIMENET, bicarbonates, CCS

Contents

1 Introduction

Anthropogenic pollution is leading to disastrous consequences for the planet, posing a serious risk to the living species that inhabit it, including human beings. Acidification of the seas, greenhouse gases, soil erosion, are all issues that are being sought to be resolved in order to limit the massive damage already caused. The Paris Agreement demands of the states that sign it a commitment to limit the global average temperature increase to well below 2 degrees Celsius. To meet this demand, it is necessary to decrease carbon dioxide emissions quickly and significantly, but at the same time there is a pressing need to devise a technology and methodology for removing the CO_2 already present in the atmosphere.
LIMENET in this sense industrialises the geological carbon cycle by capturing CO_2 in the atmosphere through a proprietary technology covered by several patents. Carbon dioxide is absorbed from the atmosphere within a process that produces calcium bicarbonate ($Ca(HCO_3)_2$), and then stored. This paper analyses the potential and characteristics of one of the storage methods: deep sea discharge. We will carry out fluid-dynamic simulations of the bicarbonate discharge cycle, analysing the distribution of the saturation state of water Ω to ensure that carbon dioxide reformation does not occur, based on studies such as Ries et al. [8] and Hartmann et al. [4].

1.1 LIMENET technology

Many carbon storage processes already occur naturally on Earth and have kept the balance of our atmosphere stable for millennia. The largest store of carbon dioxide on our planet are the seas and oceans, which have already stored up to 20-30% of the anthropogenic emissions emitted so far.
The process is simple: the ocean captures carbon dioxide and neutralises its acidity by dissolving carbonate rocks. This chemical reaction is the so-called **weathering** of limestone or weathering of carbonate rocks:

$$CO_2 + H_2O + CaCO_3 \rightarrow Ca^{2+} + 2HCO_3^- \tag{1}$$

This cycle, however, is too slow to keep up with humans' ever-growing emissions, as it would take hundreds of thousands of years to revert the balance to pre-industrial levels.As of now, the sea finds itself incapable of balancing the excessive intake of carbon dioxide, also causing a steep growth in the sea's acidity level, endangering the ecosystem and marine life itself.
LIMENET has developed a technology that allows to accelerate the weathering of limestone and ultimately create industrial plants able to absorb CO_2 from air directly from exaust streams before they reach our atmosphere and store them in seawater in form of calcium bicarbonates. Since the complete explanation of the process is beyond the goals of this report, it will be reported only a synthesis:

- **Calcination and slaking**
  First, feedstock limestone $CaCO_3$ is split into CaO (quicklime) and CO_2 through thermal decomposition inside an electric furnace powered by renewable energy. Quicklime is then hydrated to obtain slaked lime $Ca(OH)_2$.

- **CO_2 abatement**
  The obtained slaked lime is used to remove carbon dioxide produced by calcination. The process takes place in the LIMENET reactor, mixing CO_2 and $Ca(OH)_2$ into seawater:

  $$Ca(OH)_2 + 2CO_2 \rightarrow Ca(HCO_3)_2 \tag{2}$$

  The reaction balancing ensures that only half of the slaked lime is needed to completely process all the carbon dioxide, leaving the other at the disposal for the downstream carbon sequestration, that can be performed via carbonatation, precipitation or direct air capture systems.

1.2 The storage

At the end of the carbon dioxide removal process, it is necessary to develop a technique for storing the calcium bicarbonate in solution. The procedure must:

- to prevent, over time, the occurrence of **secondary production**, i.e. the reformation of carbon dioxide from the produced calcium bicarbonate;

- to be alert to the possible **impacts on the environment** of discharge, especially marine flora and fauna;

- to avoid the **re-drafting** of water discharged from the plant;
- to present **no important technological challenges** and **sustainable implementation costs**.

Different alternatives have been considered in this regard, which will be briefly reviewed in the following sub-chapters.

1.2.1 Microtunneling

Microtunnelling (figure 1) is a no-dig drilling and jacking technology, suitable for the construction of microtunnels (or small-diameter tunnels) in which to install pipelines for the transport of fluids, cables and/or services in general. It allows the underground crossing of roads, railways, watercourses, areas subject to environmental protection, archaeological areas, coastal landings, man-made areas, etc., without the need for open-cut excavations (in trenches). In the specific problem, assuming that we want to size the discharge system to support the flow rates emitted by a TLR8 system, the pipe diameter would have to be about 17 metres wide. In addition to the difficulty of finding a suitable site for microtunnelling, the cost and size of the project make this choice impractical, and it was therefore decided to discard it.

Figure 1: Simplified image of the process of microtunneling: the technology allows to introduce the pipeline below the seabed, in order to discharge far from the coasts without the use of ships.

1.2.2 Surface discharge at sea

The demands made earlier in the chapter are more easily and effectively accommodated if one considers discharging the bicarbonate solution into the sea, through the use of transport vessels. The ship is fitted with the necessary equipment to buffer the solution (figure 2) using slaked lime, in order to discharge seawater at the same pH of the environment. Then, it carries out daily discharge cycles far from the coast, with a very low travel speed. The problem with this choice lies in the possible damage to marine biota, on which there is still little literature. The bicarbonate solution could jeopardise the health of calciferous organisms, which show a thickening of their shells when faced with an increase in calcium concentration.

1.2.3 Deep discharge at sea

Discharging at depth allows significantly less impact on marine biota, whether positive or negative. Through a hose, the solution can be introduced below what is called the **photic zone**, identified as that portion of the ocean where light can penetrate the water. Below this one enters the **aphotic zone**. In the figure 3 it is possible to see how, when discharging offshore, it is sufficient to go below 200 metres to avoid the photic zone. Therefore, by discharging at a depth between 500 and 1000 metres, acting conservatively, it is possible to introduce the solution into the aphotic zone through the use of a hose

Figure 2: Schematic representation of the surface discharge process: the ship is equipped with containers of CO_2 and $Ca(OH)_2$ to buffer the bicarbonate solution in order to discharge water with the same pH as the draft water.

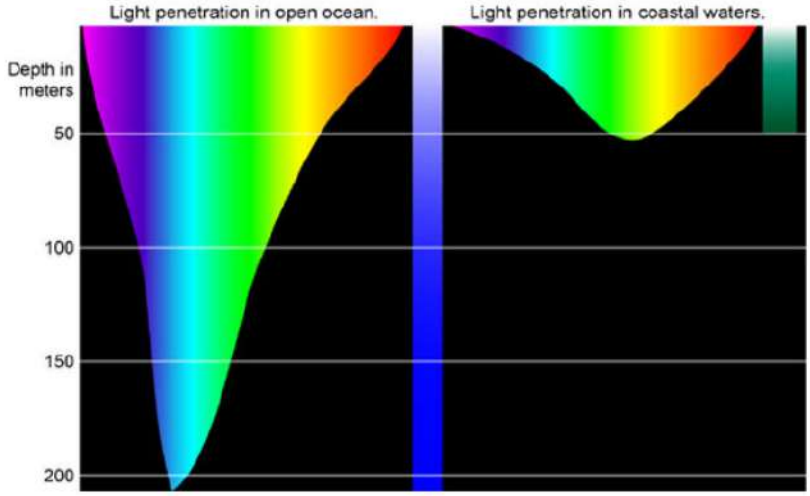

Figure 3: Light penetration in open sea and coastal waters, showing at what depths each colour of the light spectrum can penetrate. (Image taken from NOAA - National Oceanic and Atmospheric Administration via Wikimedia Commons)

connected to the system on board of the ship. The technique presented in this sub-section meets all the criteria required upstream, and is therefore the methodology adopted for this study.
According to the goals set forth in the construction of the TRL8 plant, assuming the use of a vessel capable of storing 100,000 tonnes of CO_2 annually and thus capable of producing roughly 40,000 tonnes/year of negative emissions, 18-hour discharge cycles should be set up, with an outflow of water from the discharge pipe of 13 m^3/s. The exit velocity using two 2 m diameter pipes is 2 m/s.
The aim of this project is to carry out simulations of two discharge cycles, for a total simulated time of two days, identifying the Gulf of Taranto as the area of interest (fig. 5). The point was chosen in the proximity of one of the possible construction sites of the plant.

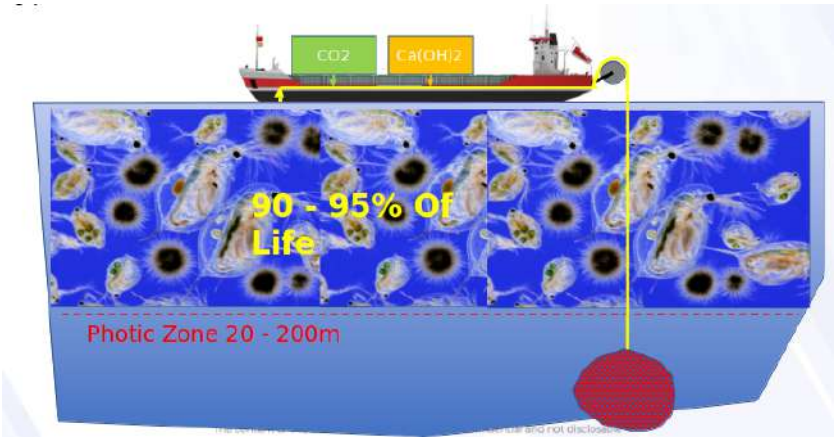

Figure 4: Schematic representation of the deep-discharge process: the difference with the surface case is the use of a hose, coiled on a shaft, to reach the discharge depth below the photic zone.

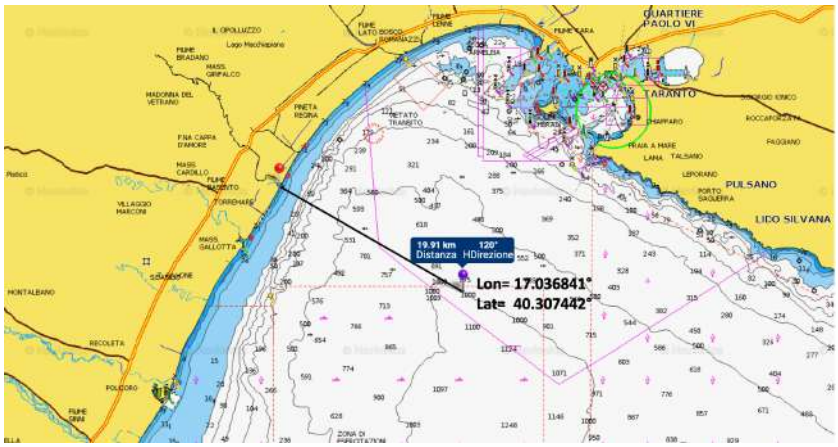

Figure 5: Coordinates of point of discharge of bicarbonate solution in the Taranto's gulf.

2 Ocean environment

In this section, the investigation philosophy of this project will be addressed and explained. In order to model the phenomenon in the best possible way, it is necessary to initially understand the scales and forces that are significant to the problem at hand. It is also necessary to identify the quantities of the simulated environment that become part of the equations, as well as the chemistry of the problem, being a solution of bicarbonate ions released in water. The chapter will be structured as follows:

- **Coriolis force and stratification effect**, in which the effect of volume forces in the specific problem will be evaluated;
- **Physical quantities**, in which the typical quantities of the ocean environment, such as temperature, salinity, density, viscosity, etc., will be reviewed.
- **Chemistry**, in which the carbon cycle will be briefly exposed, in order to define the most accurate and computationally efficient model.

2.1 Coriolis force and stratification effect

In normal engineering applications where fluid dynamic simulations are required, the effect induced by the rotation of the planet earth is generally neglected. To assess the scale at which the earth's rotation becomes an important factor in the evolution of the fluid in motion, referring to Roisin [10], we consider the term

$$\epsilon = \frac{2\pi U}{\Omega L} \tag{3}$$

where U and L mean the characteristic speed and length of the problem, respectively, while Ω represents the environmental rotation rate and is equal to $7.2921 \times 10^{-5}\ s^{-1}$.
The term ϵ thus represents the ratio of the Earth's rotation period to the time taken by a particle to cover distance L at speed U. If $\epsilon \leq 1$, the effect of the earth's rotation is considered significant. In the problem under consideration, a discharge jet with an exit velocity of $2m/s$ is simulated, considering as domain a cubic portion of sea with side 1 km: by inserting the data in the equation 3, we obtain that $\epsilon \approx 172$, thus concluding that the effect induced by the Coriolis force is negligible in the problem under consideration.

The second contribution to be examined is the stratification of the water column. In the ocean environment, water masses of different densities, due to differences in temperature, salinity and pressure, interact with each other, generally arranging themselves in a stratified structure that corresponds to the lowest potential energy state. Disturbing elements in the system such as currents, wave motion or temperature variations promote the mixing of water masses, generating phenomena such as upwelling currents, which are essential for a constant flow of nutrients to the surface layers, which are rich in living organisms. In order to examine the impact of stratification in the modelling of a problem, a *sigma* coefficient [Roisin [10]] has been defined, analogous to the Coriolis force. The physical meaning of *sigma* represents nothing more than the ratio between the kinetic and potential energy of the system:

$$\sigma = \frac{\frac{1}{2}\rho_0 U^2}{\Delta\rho g H} \tag{4}$$

where $\Delta\rho$ represents the characteristic density change of the fluid, H the characteristic depth of the problem. If $\sigma \leq 1$, kinetic energy is not able to predominantly affect the momentum field. Therefore, stratification is important for the correct modelling of the momentum field. In our specific case, the percentage density difference was calculated between 0 and 500 metres using the density formula of Zeebe et al. [14], yielding a 16% difference; U is set equal to 2 as above, while $H = 500\ m$ as the selected input point, yielding $\sigma \approx 2.5 \times 10^{-3}$. It must therefore be concluded that the stratification effect is to be considered important, and a suitable model must therefore be chosen to describe the buoyancy and stratification phenomena of the portion of the sea considered. In chapter 3, the **approximation of Boussinesq**, fundamental for the simulation of buoyancy phenomena, will be introduced.

2.2 Physical Quantities

In this chapter, we will briefly explain the physical quantities that characterise the marine environment, predominantly affecting water density, which is fundamental for modelling stratification effects. In

particular, it will be shown how these quantities generally evolve as depth changes. In addition, the correct units and scales for each quantity will be defined, so that the data and results reported can be interpreted correctly.

2.2.1 Pressure

The pressure at depth h, due to the weight of the water column of height h, is called **hydrostatic pressure**, and can be expressed according to the formula

$$\Delta p = \rho g h \tag{5}$$

where Δp corresponds to the pressure difference between sea level and a point at depth h. The pressure increases with depth at a rate of about 1 $dbar/m$: in literature it is usual to measure depth precisely by virtue of this rate. In fact, to indicate a depth of 1000 m, the term 1000 $dbar$ is often used. The increase in pressure leads to two consequences of interest to our problem:

- changes, albeit small, in the density (eq. 8);
- a greater quantity of dissolved gas, since the solubility of a gas increases with pressure (fig. 6) and with decreasing temperature.

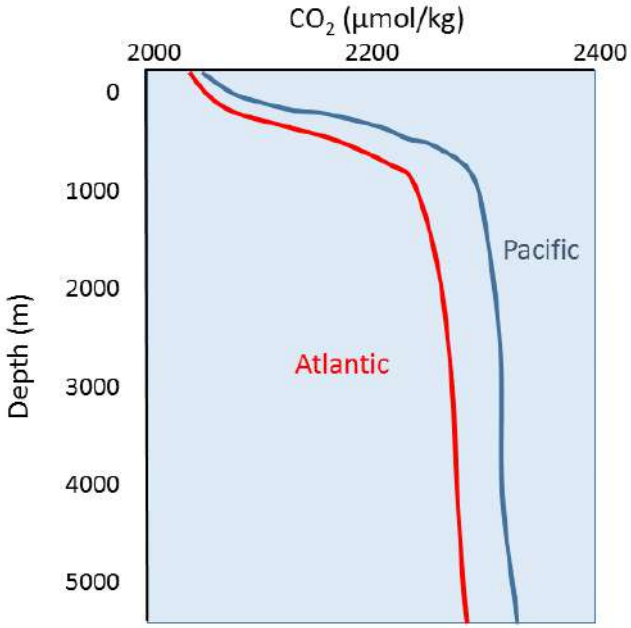

Figure 6: Representative CO_2 profile for atlantic and pacific oceans. Image taken from Webb [7]

2.2.2 Temperature

Ocean temperature varies primarily with depth and latitude, which determine how much heat a given portion of the oceans receives from the sun. As depth increases, the distance from a heat source leads to a progressive decrease in temperature. An indicative temperature profile can be seen in figure 7. It should also be noted how the temperature profile varies with latitude, due to the different exposure to the sun. In the profiles it is possible to observe a first layer of water at constant temperature, called the **mixed layer**, stirred by wave motion, currents and winds. Below this is, before a deep zone with strong thermal stability, a **thermocline**, i.e. a zone with a rapid decrease in temperature over a narrow range of depths.

The collaboration with the Euro-Mediterranean Centre on Climate Change (CMCC) has allowed the use of specific data on the marine environment in the Gulf of Taranto area. With regard to the temperature profile, in figure 8 the temperature values (in degrees Celsius) at varying depth and time,

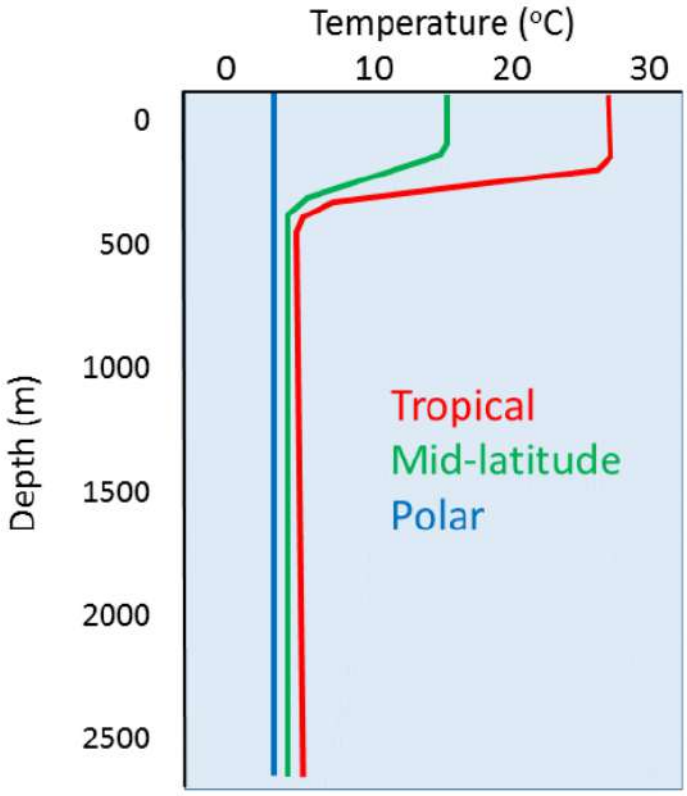

Figure 7: Representative temperature profile for different latitudes. Image taken from Webb [7]

over the course of a day, are expressed. It should be noted that we refer, as a temperature scale, to the **potential temperature**, widely used in oceanography, which is to be expressed as the temperature a sample would have if brought, by an adiabatic process, to the reference pressure. The potential temperature is used in any environment where a stratified fluid is to be studied, as it gives a measure of the stability of the fluid due to stratification, providing an indication of the possibility of convection and mixing between layers.

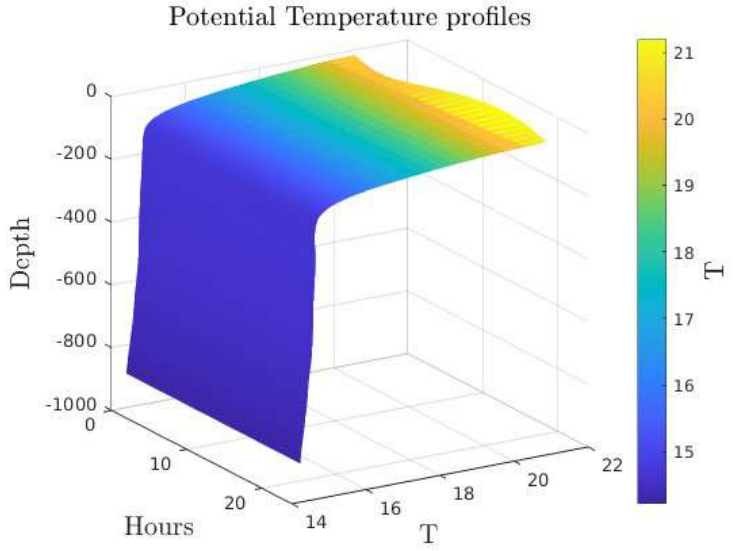

Figure 8: Hourly sea temperature profiles in the Gulf of Taranto area. Data provided by the Copernicus Marine Data Store, owned by CMCC.

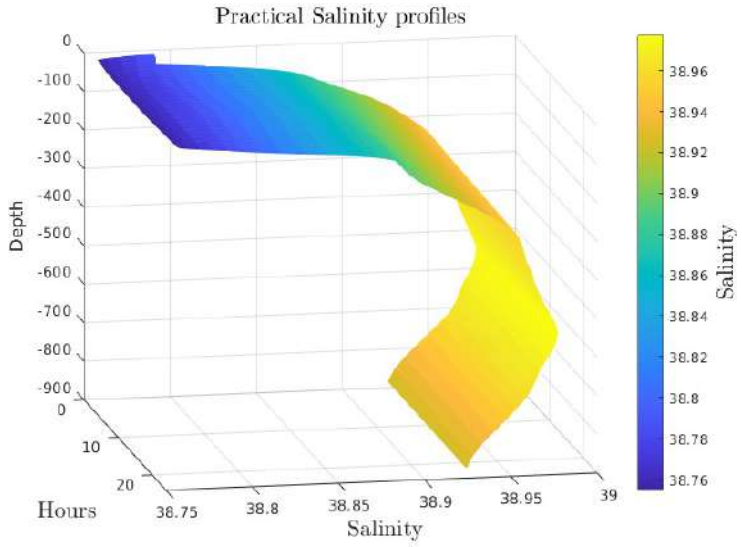

Figure 9: Hourly profiles of sea salinity in the Gulf of Taranto area. Data provided by the Copernicus Marine Data Store, owned by CMCC.

2.2.3 Salinity

Salinity is a measure of the amount of salts and ions dissolved in a seawater sample. It is usually expressed in g/Kg of solution, and is contributed by many different substances dissolved in water, including sodium, chloride, calcium, potassium, magnesium, sulphates. These ions make up more than 99% of the total salinity and are termed **conservative ions**, as their relative proportions in water remain constant[1], and salinity varies mainly as a result of removal or addition of fresh water by precipitation or evaporation. Salinity can vary between 33 and 40 g/Kg depending on latitude and particular regional conditions, such as in the Mediterranean Sea, where there is a higher salinity (figure 9) than the global average of 35 g/Kg.
Salinity mainly affects the density of water: the greater the amount of dissolved salts, the greater the density of the water sample.

2.2.4 Density

The density of water increases, as mentioned in previous chapters, with decreasing temperature, increasing salinity and pressure (i.e. with depth). The most pronounced effect is given by temperature and salinity, while pressure, since water is an incompressible fluid, contributes significantly less to density changes. In fact, the density profiles (figure 10) have a very similar physiognomy to the temperature profiles seen in figure 7: after the **mixed layer**, there is a rapid increase in density that characterises a zone of ocean defined as the pycnocline, which is considered to be almost coincident with the **thermocline** seen in the 2.2.2 section. After the pycnocline, the density increases slightly with increasing depth, due to the effect of pressure and salinity.
The equation of state for calculating density in this project is defined as a function of temperature T_C (in Celsius), pressure difference p (in bar) relative to sea level, and salinity S (in grams per kilo), using the formula given by Zeebe et al. [14]. Initially, the density of *pure water* is calculated, i.e. without the contribution from salinity (S=0):

$$\begin{aligned}\rho_{pw} = 999.842594 + 6.793952 \times 10^{-2}\ T_C - 9.095290 \times 10^{-3}\ T_C^2 + \\ 1.001685 \times 10^{-4}\ T_C^3 - 1.120083 \times 10^{-6}\ T_C^4 + 6.536332 \times 10^{-9}\ T_C^5\end{aligned} \tag{6}$$

Then, the seawater density at one atmosphere, i.e. $p = 0$, is computed as:

$$\rho_{st} = \rho_{pw} + AS + BS^{3/2} + CS^2 \tag{7}$$

[1]This characteristic is less present in coastal areas where phenomena such as river mouths alter the proportions, even if slightly.

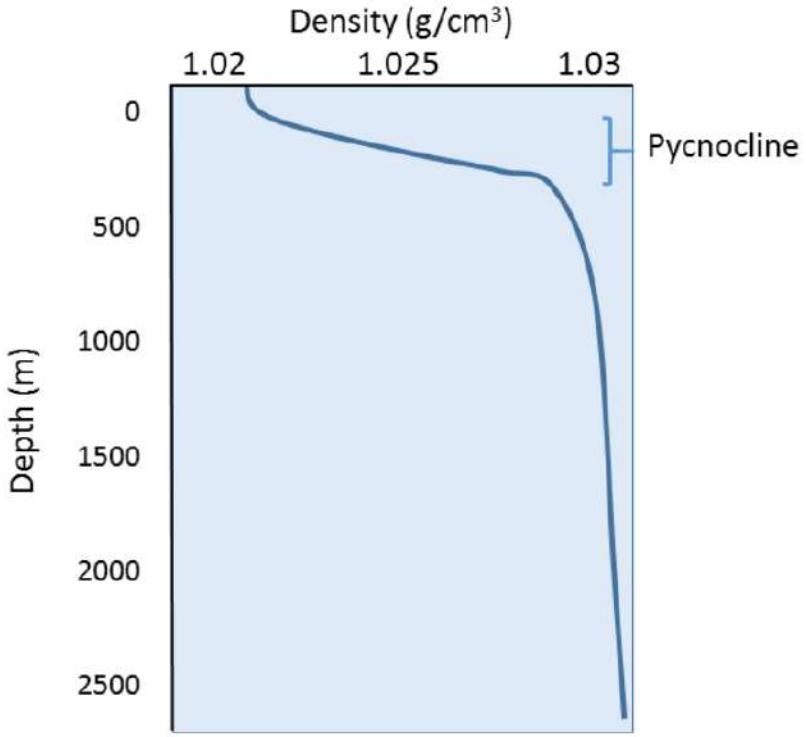

Figure 10: Representative density profile. Image taken from Webb [7]

where

$$A = 8.24493 \times 10^{-1} - 4.0899 \times 10^{-3}\ T_C + 7.6438 \times 10^{-5}\ T_C^2 - 8.2467 \times 10^{-7}\ T_C^3 + 5.3875 \times 10^{-9}\ T_C^4$$
$$B = -5.72466 \times 10^{-3} + 1.0227 \times 10^{-4}\ T_C - 1.6546 \times 10^{-6}\ T_C^2$$
$$C = 4.8314 \times 10^{-4}$$

Finally, the density is calculated by adding the effect of pressure as:

$$\rho_w = \rho_{st}/(1 - p/K_{stp}) \tag{8}$$

where

$$\begin{aligned}
K_{pw} =& 19652.21 + 148.4206\ T_C - 2.327105\ T_C^2 + 1.360477 \times 10^{-2}\ T_C^3 - 5.155288 \times 10^{-5}\ T_C^4 \\
K_{st} =& K_{pw} + S(54.6746 - 0.603459 T_C + 1.09987 \times 10^{-2}\ T_C^2 - 6.1670 \times 10^{-5}\ T_C^3) + \\
& S^{3/2}(7.944 \times 10^{-2} + 1.6483 \times 10^{-2}\ T_C - 5.3009 \times 10^{-4}\ T_C^2) \\
K_{stp} =& K_{st} + p(3.239908 + 1.43713 \times 10^{-3}\ T_C + 1.16092 \times 10^{-4}\ T_C^2 - 5.77905 \times 10^{-7}\ T_C^3) \\
& + pS(2.2838 \times 10^{-3} - 1.0981 \times 10^{-5}\ T_C - 1.6078 \times 10^{-6}\ T_C^2) + 1.91075 \times 10^{-4} pS^{3/2} \\
& + p^2(8.50935 \times 10^{-5} - 6.12293 \times 10^{-6}\ T_C + 5.2787 \times 10^{-8}\ T_C^2) + p^2 S(-9.9348 \times 10^{-7} \\
& + 2.0816 \times 10^{-8}\ T_C + 9.1697 \times 10^{-10}\ T_C^2)
\end{aligned}$$

2.2.5 Viscosity

Viscosity μ is defined as the momentum exchange coefficient. Similarly to what was shown in 2.2.4, by referring to the equations given in [11], we use Millero's relation [5] to calculate μ_w as a function of temperature and salinity. Defining the viscosity of distilled water $\mu_{20} = 1.002 \times 10^{-3}$, we calculate the viscosity of *pure water* (i.e. $S = 0$) as:

$$\log\left(\frac{\mu_{pw}}{\mu_{20}}\right) = (1.1709(20 - T_C) - 0.001827(T_C - 20)^2)/(T_C + 89.93) \tag{9}$$

Finally, the viscosity of seawater is calculated by adding the chlorinity dependence, which can be derived from salinity via the equation 10:

$$Cl = \frac{\rho_w S}{1806.55} \tag{10}$$

$$\mu_w = \mu_{pw}(1 + DCl^{1/2} + ECl) \tag{11}$$

where

$$D = 5.185 \times 10^{-5} T_C + 1.0675 \times 10^{-4}$$
$$E = 3.300 \times 10^{-5} T_C + 2.591 \times 10^{-3}$$

2.3 Chemistry

In this chapter, the chemistry aspects of the problem will be analysed. The CO_2 cycle, the concept of **Dissolved Inorganic Carbon** and alkalinity will be briefly explained. These concepts are cornerstones for setting up the system of equations that allows the calculation of carbonate speciation at equilibrium, and consequently the saturation constant Ω, the discriminating value for considering the possibility of calcium carbonate reformation, with consequent release of CO_2 into the water, thus failing the storage process.

2.3.1 The carbonate system

Several gases are dissolved within the ocean: the most abundant are oxygen, carbon dioxide and nitrogen. These play a fundamental role in the sustenance and proliferation of marine life, in processes such as biotic respiration, nutrient production and algae photosynthesis. In this section, only the chemical reactions that transform carbon dioxide will be exposed, as they determine the conditions under which CO_2 dissolved in a bicarbonate solution can be successfully stored.
In water, carbon dioxide exists in the form of aqueous carbon dioxide $CO_{2(aq)}$, bicarbonate ion HCO_3^- and carbonate ion CO_3^{2-}. Carbon dioxide is exchanged with the atmosphere, containing $CO_{2(g)}$ in gaseous form, according to the formula:

$$CO_{2(g)} \overset{K_0}{\rightleftharpoons} CO_2 \tag{12}$$

where K_0 is the solubility constant, depending on salinity and temperature.
Carbonates, at equilibrium, can then speciate as:

$$CO_{2(aq)} + H_2O \overset{K_1}{\rightleftharpoons} HCO_3^- + H^+ \overset{K_2}{\rightleftharpoons} CO_3^{2-} + 2H^+ \tag{13}$$

with K_1 and K_2 being the equilibrium constants defined as:

$$K_1 = \frac{[HCO_3^-][H^+]}{[CO_2]} \tag{14}$$

$$K_2 = \frac{[CO_3^{2-}][H^+]}{[HCO_3^-]} \tag{15}$$

The sum of the three forms of carbon dioxide identifies a quantity defined as **Dissolved inorganic carbon**:

$$DIC = [CO_2] + [HCO_3^-] + [CO_3^{2-}] \tag{16}$$

While DIC is a measurement that tracks the amount of carbonates contained in water, **Total Alkalinity** (TA) quantifies the electrical charge of the water sample as:

$$TA = [HCO_3^-] + 2[CO_3^{2-}] + [B(OH)_4^-] + [OH^-] - [H^+] + \ minor\ components \tag{17}$$

This results in a system of 4 equations (eq. 14, 15, 16, 17) in 6 unknowns ($[HCO_3^-]$, $[CO_3^{2-}]$, $[CO_2]$, $[H^+]$, DIC, TA). It is then possible to solve the system[2] if at least 2 quantities are known. In the present problem, DIC and pH were plotted, as they are easy to draft from the *Copernicus Marine Data Store*,

[2]The public matlab code of [14] was used in postprocessing to solve the system.

and to measure as discharge conditions.

So far, the carbonate system has been presented at equilibrium, reporting reactions and associated equilibrium constants. However, it must be considered how the present system is inherently dynamic, responding to external perturbations with a return to equilibrium conditions according to relaxation times that vary depending on the reaction considered, temperature, pH, DIC and pressure. A detailed explanation of this phenomenon is beyond the scope of this report and is illustrated in Chapter 2 of Zeebe's book [14]. The process with the longest relaxation time can be found in the reaction between CO_2 and water to form HCO_3^-, with relaxation times of about 10 s for seawater at standard pH and DIC. Characteristic simulation times, being of the order of minutes, thus allow the carbonate system to be considered at equilibrium, decreasing computational costs.

2.3.2 Saturation state of seawater

The calculation of carbonate speciation makes it possible to assess the saturation state of seawater Ω, expressed as

$$\Omega = \frac{[Ca^{2+}_{sw}] \times [{CO_3^{2-}}_{sw}]}{K^*_{sp}} \tag{18}$$

where K^*_{sp} is the stoichiometric solubility product were used, while $[Ca^{2+}_{sw}]$ and $[{CO_3^{2-}}_{sw}]$ are the concentrations of calcium and bicarbonate ions in water. The saturated state of the water therefore depends on the *in situ* conditions of the water and, in particular, on the concentration of bicarbonate ions, as the calcium concentration does not vary significantly, and is essentially dependent on salinity. The calculation of Ω makes it possible to assess whether the solution is supersaturated ($\Omega > 1$) or undersaturated ($\Omega < 1$), allowing conclusions to be drawn, for example, on the corrosive action of the water on calcifying organisms, which see the dissolution of shells accentuated as Ω decreases (Ries [8]).

The main objective of this analysis, as already mentioned in chapter 1, is the analysis of the distribution of the state of water saturation during discharge cycles, in the sea area considered. Determining a Ω value allows one to assess the stability of carbonates over time, establishing whether or not abiotic production of carbon dioxide can occur. The literature on this subject (Hartmann et al. [4], Moras et al. [6]) defines $\Omega \approx 5$ as the saturation limit value to avoid the formation of CO_2. The results of these two studies were also confirmed by an analysis carried out as part of the Limenet project (Hyrogas [12]), in which the stability of bicarbonates over time in seawater samples at different CO_2 water and sample dilution ratios was studied.
As can be seen in figure **??**, at a dilution ratio of 1:20 there is no appreciable decrease in TIC, which would indicate a reformation of carbon dioxide within the water sample. At these dilution conditions and water-carbon dioxide ratio, the saturation state is about 3.7, a value in agreement with the available literature.

In order to draw relevant conclusions and observations from the simulations carried out, a water saturation state of 5 will be assumed as the limit value for the project under consideration.

For the calculation of the saturation state, referring to eq. 18, it is needed to compute:

- calcium concentration of seawater, retrieved from literature (Appendix 12 Zeebe [14]) and kept fixed at 0.4121 g/Kg;
- bicarbonate concentration, computed from DIC via speciation of carbonate, as illustrated in the previous chapter;
- K^*_{sp}, including the effect of pressure, using the formulas in Appendix 10 and 11 of Zeebe [14].

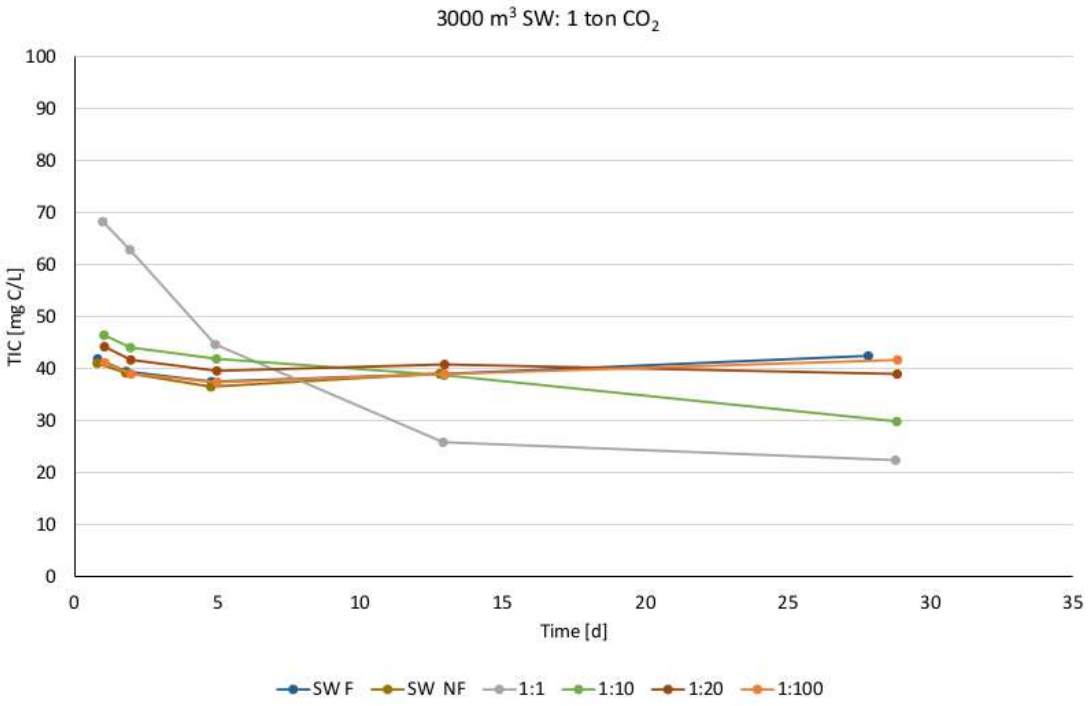

Figure 11: Study of the *Total inorganic carbon* (TIC) in a sample with a water-carbon dioxide ratio of 3000 m^3 : 1 *ton* and a dilution ratio ranging from 1:1 to 1:100. Image taken from Hyrogas technical report [12]

3 Equations

Solving any fluid dynamic problem requires solving the Navier-Stokes equations (eq. 19 and 20), presented here for an incompressible fluid in differential form, using Einstein's notation for subscripts. In light of the characteristics of the problem and the observations made in chapter 2 about the importance of stratification effects, the Boussinesq approximation, which can be further explored in Rieutord [9], was introduced. With this approximation, density is considered constant except in the computation of volume forces, where density varies with temperature[3], which then requires an equation describing its diffusion and convection within the simulated domain (eq. 21). Finally, to describe the distribution of DIC and pH, the associated equations are the same as those describing the transport of a passive scalar (eq. 22): given the conditions of the problem, therefore, these are formally identical to those for temperature, given the absence of source terms for each of these three quantities.

$$\frac{\partial u_i}{\partial x_i} = 0 \tag{19}$$

$$\frac{\partial u_i}{\partial t} + \frac{\partial u_i u_j}{\partial x_j} = -\frac{1}{\rho_0}\frac{\partial p'}{\partial x_i} + \frac{\partial}{\partial x_j}\left(\frac{\mu}{\rho} S_{ij}\right) + \frac{\rho'}{\rho_0}\mathbf{g} \tag{20}$$

$$\frac{\partial T}{\partial t} + \frac{\partial u_j T}{\partial x_j} = K\nabla^2 T \tag{21}$$

$$\frac{\partial Y_i}{\partial t} + \frac{\partial u_j Y_i}{\partial x_j} = D_i \nabla^2 Y_i \tag{22}$$

where

$$p' = p - p0, \quad \rho' = \rho_w - \rho_0, \quad \rho_w = \rho_w(S,T), \quad \mu = \mu_w(S,T)$$

Within the FORTRAN code, dimensionless equations were included with respect to velocity and characteristic length. All the characteristic quantities, like temperature, salinity, pH, density etc.. are referred to the injection conditions, and can be visualized in Table 1. It has to be noted how, for the DIC value,

[3]In the oceanic environment, as explained in the chapter 2.2.4, density also varies with salinity and pressure (eq. 8)

U	$2\ m/s$
L	$2\ m$
T_0	$20\ ^\circ C$
S_0	$38\ g/Kg$
p	$50\ bar$
ρ_0	$1029\ Kg/m^3$
μ_0	$1.078 \cdot 10^{-3}\ N/m*s$
pH	8.11
DIC	$10.187\ mol/m^3$

Table 1: Reference quantities for the adimensionalization of the equations.

the computation of the injection value is based upon the assumption of a discharge of CO_2 with a ratio between m^3 of water per ton of carbon dioxide of 3000:1.

$$u_i^* = u_i/U, \quad x_i^* = x_i/L, \quad t^* = tU/L, \quad \rho^* = \rho/\rho_0, \quad p^* = p/(\rho_0 U^2), \quad T^* = T/T_0, \quad \mathbf{g}^+ = \mathbf{g}/\mathbf{g}_0 = (0,0,1)$$

$$\frac{\partial u_i^*}{\partial x_i^*} = 0 \tag{23}$$

$$\frac{\partial u_i^*}{\partial t^*} + \frac{\partial u_i^* u_j^*}{\partial x_j^*} = -\frac{\partial p'^*}{\partial x_i^*} + \frac{\partial}{\partial x_j^*}\left(\frac{1}{Re} S_{ij}^*\right) + \frac{1}{Fr^2}\rho'^* \mathbf{g}^* \tag{24}$$

$$\frac{\partial T^*}{\partial t^*} + \frac{\partial u_j^* T^*}{\partial x_j^*} = \frac{1}{RePr}\nabla^2 T^* \tag{25}$$

$$\frac{\partial Y_i^*}{\partial t^*} + \frac{\partial u_j^* Y_i^*}{\partial x_j^*} = \frac{1}{ReSc_i}\nabla^{2^*} Y_i^* \tag{26}$$

where

$$Re = \frac{\rho_0 U L}{\mu_0}, \quad Fr = \frac{U}{\sqrt{Lg}}, \quad Pr = \frac{K}{\nu}, \quad Sc_i = \frac{D_i}{\nu}$$

With $Re,\ Fr,\ Pr,\ Sc_i$ being respectively Reynolds, Froude, Prandtl and Schmidt numbers. Using these reference quantities, in table 2 the dimensionless numbers are:

Re	$3.8 \cdot 10^6$
Fr	0.45
Pr	6.97
Sc	1

Table 2: Dimensionless parameters for the present project

For the Schmidt number, with DIC and pH being the transported passive scalars, the diffusion coefficient has been fixed equal the water viscosity, resulting in a unitary dimensionless coefficients within the transport equations.

4 Computational aspects

The following chapter is entirely devoted to the code used, with the aim of providing an essential and complete understanding of the fundamental tool for this project: the solver code. For the current study, a FORTRAN code developed by Professor A. Abbà of the Polytechnic University of Milan was used. The code uses a finite difference method to perform Large Eddy Simulations (LES) on a *staggered grid*. The simulated domain consists of a 1 km side portion of the sea with a nonuniform orthogonal mesh, where on the side defined as the "*inlet*", cells have been selected to simulate the input of the bicarbonate solution. Throughout this chapter, the fundamental features and concepts that make up the architecture of the code used, from the solving method to the parallelization approach, will be briefly explained, concluding with the initial and boundary conditions for solving the equations presented in chapter 3. For more on the elements that constitute it, see Ferziger [2].

4.1 Finite differences

Finite-difference methods constitute a fundamental numerical approach employed in fluid dynamic simulations, playing a crucial role in analyzing and solving the partial differential equations governing fluid behavior. The discretization of the mass, momentum and transport conservation equations (chapter 3) is done by partitioning the domain into a finite computational grid, in which each cell represents a discrete entity.

In finite-difference methods, discretization takes place in a *structured grid*, that is, a grid in which each node can be considered the origin of a local coordinate system with axes coincident with the grid axes. It follows that each cell can be uniquely identified with indices (i, j, k) in three dimensions.
Taking a generic transport equation as a reference (a general and immediate example can be found in eq. 22), the discretization of the convective term within the code is performed by adopting a *central difference* scheme, in which the quantity $\frac{\partial uY}{\partial x}$, which for convenience of notation we will call $\frac{\partial \phi}{\partial x}$, can be approximated as

$$\frac{\partial \phi}{\partial x} = \frac{\phi_{i+1} - \phi_{i-1}}{x_{i+1} - xi - 1} \tag{27}$$

where subscripts denote, from the i-th cell, the ϕ quantity known in the i+1-th and i-1-th cells and the coordinates relative to those cells. The approximation introduces an error, intrinsic to the operation, called *truncation error*. The truncation error depends on two elements:

- the distance between two cells Δx. The approximation converges to the exact value of the derivative with an error that is proportional to $(\Delta x)^m$, where m denotes the largest exponent in the expression of the truncation error, which for a central differences scheme is equal to 2.
- the derivatives of the variable of interest. Since we therefore have to simulate a jet, it is reasonable to assume that the gradients are nonuniform along the domain: it follows that the truncation error is also nonuniform. To solve this problem, we refine the grid in areas of the domain where larger gradients are witnessed, increasing the cell size where, on the other hand, a more constant pattern of the variables of interest is expected. With this approach, one is able to obtain an almost homogeneous distribution within the domain.

Discretization of equations by methods such as central difference can lead to mathematically correct but physically inconsistent pressure distributions. This is referred to in the literature as the *checkerboard problem* (Ferziger [2], pg. 196). To solve the problem, a *staggered grid* (Harlow [3]), is used, in which the pressure and velocity values are evaluated on two different grids, staggered in fact, such that the cell center of the grid relating to pressure coincides with the face of the grid assigned to velocity, and vice versa.

4.2 Solution of Navier Stokes equations

Solving the unsteady Navier-Stokes equations aims to calculate, for each computational cell and for each instant of time, the three components of velocity and pressure. The problem is complicated by the lack of an independent equation for pressure, whose gradient contributes to each of the three momentum equations. The mass conservation equation, especially in the incompressible case, is more of a kinematic constraint on the velocity field rather than an equation describing the dynamics of the phenomenon.

To solve the problem, a pressure field is constructed such that the velocity results in zero divergence (eq. 19). In this way the pressure is defined minus a constant, which can simply be set at a point in the domain, since the quantity of interest in solving the momentum equations is simply its gradient. The equation for calculating the pressure field can be derived by calculating the divergence of (20) and eliminating the terms using (19): the resulting equation is called **Poisson's equation**.
Implementing this resolution philosophy means using a method defined as *projection method*, in which:

- the momentum equation is solved, using the pressure term related to the previous time step. In this way a provisional velocity $\mathbf{u}^*$ is calculated;
- $\mathbf{u}^*$ is used to solve the Poisson equation and updating the velocity to make it zero divergence, yielding $\mathbf{u}$.

Within the code used, the momentum equation is advanced in time using an explicit 3-step *runge Kutta method*, an iterative method of which a single-step schematic succession is given:

- $\mathbf{u}^*$ is computed:
$$\mathbf{u}^* = \mathbf{u}_{t-1} + RHS_{t-1} - \nabla p_{t-1} \cdot \Delta t \tag{28}$$
where $t-1$ indicates the previous time-step, Δt the temporal increment between a time-step and the next one and RHS the known terms of the momentum equation, like the stress tensor, the gravity contribute and the subgrid terms due to the LES approach;
- Divergence of $\mathbf{u}^*$ is calculated;
- Solving the Poisson's equation:
$$\nabla^2 p_t = \frac{\nabla \cdot \mathbf{u}^*}{\Delta t} \tag{29}$$
- Finally, update the velocity:
$$\mathbf{u_t} = \mathbf{u}^* + \nabla p \cdot \Delta t \tag{30}$$

4.3 Linear system solution

The finite difference approximation produces an algebraic equation for each grid cell, linear or nonlinear depending on the presence of nonlinearity elements within the starting differential equation. The system that is generated can be written as:
$$\mathbf{A}\phi = \mathbf{Q} \tag{31}$$
where $\mathbf{A}$ is a tridiagonal matrix by virtue of the discretization scheme used, ϕ is a vector containing the variables to be calculated for each grid cell, and $\mathbf{Q}$ is a vector containing the known terms of the equations.
The numerical resolution of this system, which is large given the great number of cells within the domain, is carried out using techniques that reduce computational cost. In this specific problem, the linear system for solving (29) is made out with the use of an **Alternate Direction Implicit method** and with **Thomas Algorithm** for handling the tridiagonal matrix. The following is a brief explanation of both concepts.

4.3.1 Alternate Direction Implicit method

Solving an elliptic equation such as Poisson's equation (eq. 29) can be decomposed into three distinct and independent processes, equivalent to solving the problem along the three directions x, y, z.
Let us consider the Laplace equation for simplicity:
$$\frac{\partial^2 u}{\partial x^2} + \frac{\partial^2 u}{\partial y^2} = 0 \tag{32}$$
with the boundary conditions:
$$\begin{aligned} &u(0,y) = u(1,y) = u(x,0) = 0, \\ &u(x,1) = 1 \end{aligned} \tag{33}$$
ADI is now applied to solve the problem splitting it in three passages:

Step 1: spatial decomposition and first time step in the x direction
We divide the spatial domain into N_x intervals in the x direction and N_y intervals in the y direction, obtaining a grid $N_x \times N_y$ interior points. We define the spatial increments ($\Delta x = \frac{1}{N_x+1}$) and ($\Delta y = \frac{1}{N_y+1}$). The grid nodes are given by ($x_i = i \cdot \Delta x$) and ($y_j = j \cdot \Delta y$). We use the central difference to approximate the second derivative with respect to x.

$$\frac{\partial^2 u}{\partial x^2} \approx \frac{u(x_{i+1}, y_j) - 2u(x_i, y_j) + u(x_{i-1}, y_j)}{\Delta x^2} \tag{34}$$

By fixing $t = t^{n+\frac{1}{2}}$, we obtain the approximation ($u_{i,j}^{n+\frac{1}{2}}$ for the solution at $t^{n+\frac{1}{2}}$. The discretized equation becomes:

$$\frac{u_{i+1,j}^{n+\frac{1}{2}} - 2u_{i,j}^{n+\frac{1}{2}} + u_{i-1,j}^{n+\frac{1}{2}}}{\Delta x^2} + \frac{\partial^2 u}{\partial y^2} = 0 \tag{35}$$

We now solve this equation for $u_{i,j}^{n+\frac{1}{2}}$, by keeping j constant and using the Thomas algorithm (4.3.2).

Step 2: temporal decomposition and second time step in the y direction
After having retrieved ($u_{i,j}^{n+\frac{1}{2}}$), the equation can be solved in the y direction:

$$\frac{u_{i,j+1}^{n+1} - 2u_{i,j}^{n+\frac{1}{2}} + u_{i,j-1}^{n+1}}{\Delta y^2} + \frac{\partial^2 u}{\partial x^2} = 0 \tag{36}$$

where $u_{i,j+1}^{n+1}$ is the approximation of the solution at t^{n+1}, obtained by solving the resulting equation with constant i.

Step 3: temporal iteration
We repeat steps 1 and 2 for a desired number of time iterations or until the solution converges to some tolerance. Alternating between the x and y directions in the time steps constitutes the ADI approach. A three-dimensional version in detail would be too beyond the purposes of this technical report. For more information, see Douglas [1].

4.3.2 Algoritmo di Thomas

Approximating the equations by discretization to central differences yields a system of algebraic equations characterized by a simple structure, where each equation contains only the variables of the respective node and the two immediately following and preceding ones:

$$A_W^i \phi_{i-1} + A_P^i \phi_i + A_E^i \phi_{i+1} = Q_i \tag{37}$$

The matrix A that comes to be constructed is a tridiagonal matrix, uniquely definable through the three diagonals (A_W lower diagonal, A_P middle diagonal, A_E upper diagonal). Matrices of this type are easily solved by the Gauss elimination method. When the algorithm reaches the $i-th$ row, only A_P^i and Q_i need to be modified to compute ϕ_i as:

$$\begin{aligned} A_P^i &= A_P^i - \frac{A_W^i A_E^{i-1}}{A_P^{i-1}} \\ Q_i^* &= Q_i - \frac{A_W^i Q_{i-1}^*}{A_P^{i-1}} \\ \phi_i &= \frac{Q_i^* - A_E^i \phi_{i+1}}{A_P^i} \end{aligned} \tag{38}$$

Thomas's algorithm allows the system of equations to be solved at a computational cost proportional to n, making this approach particularly convenient and functional in terms of scalability and computational performance.

4.4 Parallelization

The size of the problem, which intends to simulate such a large portion of the sea for a time of about two days, requires an undoubtedly high computational cost. In addition to solving the system of equations with efficient and effective approaches and techniques, such as Thomas's algorithm (sec. 4.3.2) and the ADI method (sec. 4.3.1), it is possible to accelerate the resolution by the computer through MPI (*Message passing interface*) libraries and by partitioning the problem into a sequence of independent *tasks*, using the technique of **Schur's complement**.

4.4.1 MPI and Cartesian decomposition

The performance of a computer, in terms of the speed at which an algorithm is executed, can be improved in basically two ways. The first is to improve the performance of the computing unit (CPU) by improving the *clock speed*, i.e., the number of operations per second that the CPU is able to perform. Today, however, modern technologies do not allow values on the order of 10^9 GHz to be exceeded; therefore, the only viable way forward is to build systems composed of multiple CPU working simultaneously. This solution is called **parallelization**. The computing units communicate with each other to carry out the provided algorithm, which is then divided into independent or semi-independent *tasks*. In the present project, the **MPI libraries** implement a *message passing* approach to parallelization. With this method, a single program is written and executed on each processor, which performs a different process depending on the amount of data it handles and its "hierarchy" among the processes.
In MPI, relationships between processors are defined through communicators. The main communicator is **MPI_COMM_WORLD**, which assigns a number (called *rank*) to each process, allowing each to communicate by reference to its respective rank. In order to handle a problem such as the one under consideration, where the number of processes is large, an additional step is taken: a *Cartesian communicator*.
Such a technique distributes the processes on N orthogonal axes, assigning rank to each process as a set of coordinates on the Cartesian grid. In this way, the physical domain is divided into blocks, whose boundaries will coincide with those between processes on the grid.

4.4.2 Schur's complement

Given a matrix $\mathbf{M}$, divided in blocks:

$$\mathbf{M} = \begin{bmatrix} \mathbf{A} & \mathbf{B} \\ \mathbf{C} & \mathbf{D} \end{bmatrix} \tag{39}$$

the **Schur's complement** of $\mathbf{D}$ is defined as:

$$\mathbf{M/D} = \mathbf{A} - \mathbf{B}\mathbf{D}^{-1}\mathbf{C} \tag{40}$$

while the Schur's complement of $\mathbf{A}$ as:

$$\mathbf{M/A} = \mathbf{D} - \mathbf{C}\mathbf{A}^{-1}\mathbf{B} \tag{41}$$

By using the Schur's complement, a linear system in the form:

$$\begin{bmatrix} \mathbf{A} & \mathbf{B} \\ \mathbf{C} & \mathbf{D} \end{bmatrix} \begin{Bmatrix} x \\ y \end{Bmatrix} = \begin{Bmatrix} a \\ b \end{Bmatrix} \tag{42}$$

can be splitted in two independent problems:

$$\begin{cases} \mathbf{x} = (\mathbf{M/D})^{-1}(\mathbf{a} - \mathbf{B}\mathbf{D}^{-1}\mathbf{b}) \\ \mathbf{y} = (\mathbf{M/A})^{-1}(\mathbf{b} - \mathbf{C}\mathbf{A}^{-1}\mathbf{a}) \end{cases} \tag{43}$$

In the present project, this concept solves a problem that arises with the Cartesian decomposition of processes. Figure 12 illustrates the structure of a tridiagonal problem, where its domain is divided among processes through a Cartesian decomposition. The critical aspect lies in the interface values, represented as red dots, because the corresponding equations need two values (blue and green dots on the same line) belonging to two distinct processes: from the point of view of a single process, one of the two values is known, while the other is not.
To solve this problem we rearrange the matrix so that the interface points are concentrated in the last few rows (figure 13), dividing the problem into inner and interface zones.

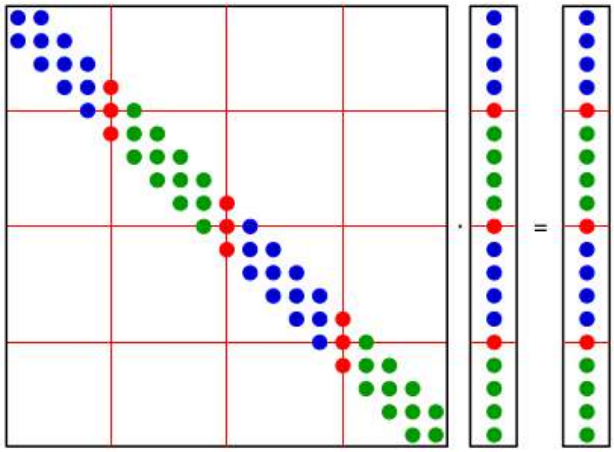

Figure 12: Tridiagonal system split between different processes. Image taken from Zanelli [13]

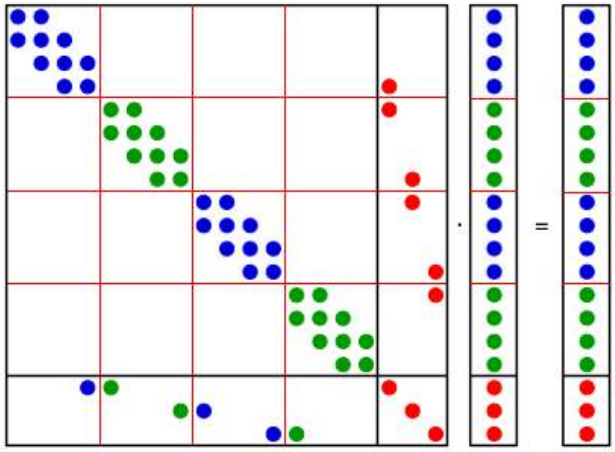

Figure 13: Tridiagonal system rearranged in order to separate its internal and interface parts. Image taken from Zanelli [13]

$$\begin{bmatrix} \mathbf{A}_{ii} & \mathbf{A}_{ie} \\ \mathbf{A}_{ei} & \mathbf{A}_{ee} \end{bmatrix} \begin{Bmatrix} \mathbf{x}_i \\ \mathbf{x}_e \end{Bmatrix} = \begin{Bmatrix} \mathbf{f}_i \\ \mathbf{f}_e \end{Bmatrix} \tag{44}$$

The matrix that is created, as visible from figure 13, is block diagonal, where the blocks of each process can be denoted as $A_{ii}^{(p)}$. Schur's complement is then computed at the beginning, only once. In fact, if the matrix $\mathbf{A}$ does not vary, the complement $\mathbf{A}/\mathbf{A}_{ii}$ is saved in the "master process" (the process with rank equal to 0). At each time instant, each process computes, using Thomas's algorithm, $\mathbf{A}_{ii}^{(p)-1} f_i^{(p)}$, since it is independent of the remaining blocks. Next, each process sends to the "master process" the respective portion of the vector $\mathbf{A}_{ei}^{(p)} \mathbf{A}_{ii}^{(p)-1} f_i^{(p)}$, which is subsequently assembled into $\mathbf{A}_{ei} \mathbf{A}_{ii}^{-1} f_i$, thus allowing $\mathbf{x}_e$ and $\mathbf{x}_i$ to be calculated as:

$$\begin{cases} \mathbf{x}_e = (\mathbf{A}/\mathbf{A}_{ii})^{-1} (\mathbf{f}_e - \mathbf{A}_{ei} \mathbf{A}_{ii}^{-1} \mathbf{f}_i) \\ \mathbf{x}_i^{(p)} = \mathbf{A}_{ii}^{(p)-1} (\mathbf{f}_i^{(p)} - \mathbf{A}_{ie}^{(p)} \mathbf{x}_e) \end{cases} \tag{45}$$

4.5 Initial conditions

Solving a time-varying system composed of differential equations as in 3 requires the definition of initial conditions, on the boundary and within the simulated domain, that can initialize the simulation.
In the present project, these conditions were imposed using data provided by the *Euro-Mediterranean*

Center on Climate Change (CMCC), thanks to which it was possible to define the fluid dynamic and geochemistry quantities of the portion of the sea under consideration, located in the Ionian Sea, precisely at coordinates $40.31N$ $17.04E$. CMCC provided data regarding:

- velocity components v_x and v_y;
- temperature T;
- salinity S;
- dissolved inorganic carbon DIC;
- pH.

For each quantity, 24-hour hourly data were provided for each depth level. Depth profiles were then extracted by averaging the data over time (figure 14). Within the code, the above profiles were imposed, constant over time.

4.6 Boundary conditions

Boundary conditions allow a finite difference problem to be solved by imposing on the boundary of the domain either the value of the quantity (Dirichlet condition) or that of the relative derivative (Neumann condition). A Neumann condition of zero value was then imposed for the pressure on all faces of the domain. As for velocity, to simulate the instability of wave motions, time-averaged quadratic deviations were computed for the same depth level, thus obtaining a profile of quadratic deviations to be fitted on one face of the domain (thus named *inlet*) as a Gaussian disturbance of amplitude equal to that of the deviation. On the remaining faces, a null Neumann condition was imposed.
As for the boundary condition that simulates and represents the input by the hose, the side of the square equivalent to the diameter of the hose of diameter 2 m was calculated, and then velocity, temperature, pH and DIC were imposed equal to those identifiable in Table 1.

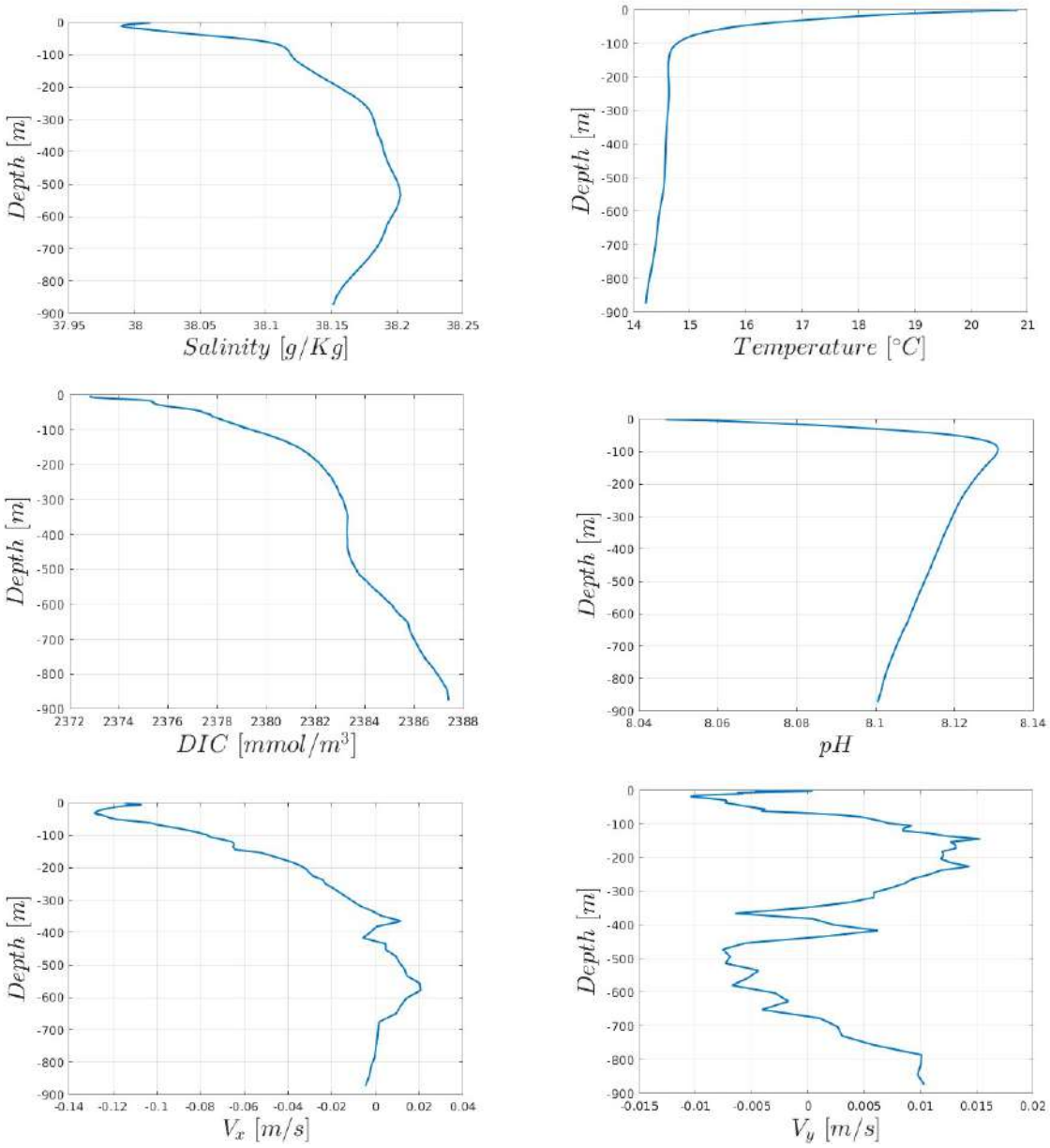

Figure 14: Profiles of the quantities of interest along the z direction, averaged over time. Data provided by CMCC

References

[1] Jim Douglas. Alternating direction methods for three space variables. *Numerische Mathematik*, 4 (1):41–63, 12 1962. ISSN 0945-3245. doi:10.1007/BF01386295. URL https://doi.org/10.1007/BF01386295.

[2] J.H. Ferziger and M. Peric. *Computational Methods for Fluid Dynamics*. Springer Berlin Heidelberg, 2012. isbn:9783642560262. URL https://books.google.it/books?id=BZnvCAAAQBAJ.

[3] Francis H. Harlow and J. Eddie Welch. Numerical Calculation of Time-Dependent Viscous Incompressible Flow of Fluid with Free Surface. *The Physics of Fluids*, 8(12):2182–2189, 1965. doi:10.1063/1.1761178. URL https://doi.org/10.1063/1.1761178.

[4] J. Hartmann, N. Suitner, C. Lim, J. Schneider, L. Marín-Samper, J. Arístegui, P. Renforth, J. Taucher, and U. Riebesell. Stability of alkalinity in ocean alkalinity enhancement (oae) approaches – consequences for durability of co_2 storage. *Biogeosciences*, 20(4):781–802, 2023. doi:10.5194/bg-20-781-2023. URL https://bg.copernicus.org/articles/20/781/2023/.

[5] Drost-Hansen W. Korson L. and Millero F. J. Viscosity of water at various temperatures. *Journal of Physical Chemistry*, 73:34, 1969.

[6] C. A. Moras, L. T. Bach, T. Cyronak, R. Joannes-Boyau, and K. G. Schulz. Ocean alkalinity enhancement – avoiding runaway $caco_3$ precipitation during quick and hydrated lime dissolution. *Biogeosciences*, 19(15):3537–3557, 2022. doi:10.5194/bg-19-3537-2022. URL https://bg.copernicus.org/articles/19/3537/2022/.

[7] Webb P. *Introduction to Oceanography*. Roger Williams University, 1st edition, 2019.

[8] Justin B. Ries, Maite N. Ghazaleh, Brian Connolly, Isaac Westfield, and Karl D. Castillo. Impacts of seawater saturation state (a=0.4–4.6) and temperature (10, 25°c) on the dissolution kinetics of whole-shell biogenic carbonates. *Geochimica et Cosmochimica Acta*, 192:318–337, 2016. ISSN 0016-7037. doi:https://doi.org/10.1016/j.gca.2016.07.001. URL https://www.sciencedirect.com/science/article/pii/S0016703716303817.

[9] Michel Rieutord. *Fluid Dynamics: an Introduction*. Springer Cham, 2014. doi:https://doi.org/10.1007/978-3-319-09351-2.

[10] Beckers J. Roisin B. *Introduction to geophysical fluid dynamics*. Academic Press, 1st edition, 2019.

[11] John H. Lienhard V. Sharqawy, Mostafa H. and Syed M. Zubair. *The thermophysical properties of seawater: A review of existing correlations and data.* Desalination and Water Treatment, 1st edition, 2010.

[12] Hyrogas SIA. Carbon storage by limenet. Technical report, Hyrogas, 2022.

[13] Tommaso Zanelli. Large eddy simulation of turbulent flows by a direction splitting solver in complex geometries. Master's thesis, Politecnico di Milano, 2018.

[14] Wolf-Gladrow D. Zeebe E. *CO_2 in seawater: equilibrium, kinetics, isotopes*. Elsevier, 1st edition, 2001.